Electronic stopping power of magnesium including inner-electron excitation

Wen-Qi Zuo,[1] Fei Mao,[1,*] Shi-Ming Li,[1] Wen-Qi Jin,[1] Rui-Da Chen,[1] Ge-Ge Xiong,[1] Cong-Zhang Gao,[2,†] Feng Wang,[3] and Feng-Shou Zhang[4]

[1]*School of Nuclear Science and Technology, University of South China, Hengyang 421001, China*
[2]*Institute of Applied Physics and Computational Mathematics, Beijing 100088, People's Republic of China*
[3]*School of Physics, Beijing Institute of Technology, Beijing 100081, China*
[4]*The Key Laboratory of Beam Technology of Ministry of Education, College of Nuclear Science and Technology, Beijing Normal University, Beijing 100875, China*

(Received 7 September 2022; accepted 11 January 2023; published 31 January 2023)

The electronic stopping power of magnesium for protons and He ions is studied by a nonequilibrium approach based on real-time time-dependent density-functional theory combined with Ehrenfest molecular-dynamics simulation. The electronic stopping power of Mg for energetic protons and He ions is calculated, and the microscopic excitation mechanism for the inner $2p$ electron of Mg and its contribution to electronic stopping power is revealed. In the low-energy range, the velocity proportionality of the electronic stopping power of Mg for protons is displayed. The low-energy stopping power of Mg for He ions displays deviations from the velocity proportionality, which is ascribed to the electronic structure of He ions that enables an additional energy-loss channel due to charge exchange. Our calculated stopping power is in a quantitative agreement with the experimental data up to the stopping maximum, and the stopping power including also $2p$-electron excitation is considerably improved compared to that with only the valence electron taken into account. Our results showed that the contribution of p-electron excitation to the electronic stopping is remarkable in the high-velocity regime. The scaling relationship $\sqrt{S_\alpha/S_H} = \overline{q}_\alpha/\overline{q}_H$ can be extended to low velocities provided that the mean steady-state charge is employed instead of assuming fully ionized charges and considering also $2p$-electron excitation of Mg.

DOI: 10.1103/PhysRevA.107.012818

I. INTRODUCTION

The study of energy deposition of charged ions traveling through materials is an active field in particle and nuclear physics. The interaction between ions and substances, such as metals [1,2], semiconductors [3,4], insulators [5,6], and liquids [7,8], is significantly important in many applied fields such as nuclear engineering [9,10], materials science [11], and radiotherapy [12]. An ion with velocity v loses energy subject to a decelerating force from the host atoms when penetrating materials, and the stopping power S is usually employed to quantify this energy loss, which is defined as the energy loss from the projectile to the target system per unit path. The S can be partitioned into two parts: electronic stopping power S_e due to electronic excitations by inelastic collisions between ions and host electrons, and nuclear stopping power S_n ascribed to atomic displacement by elastic collisions between ions and host nuclei [13–15].

The low-energy S_e of materials has been extensively studied in the past decades [16–21]; the electronic structure and details in the density of states (DOS) of the irradiated substance become important for the electronic energy loss of slow ions. Therefore, the study of the underlying physical mechanism of the electronic energy loss of slow ions traveling in materials has attracted great attention [11,22,23]. Many theoretical models [24–28] have been developed to understand the physical mechanism for S_e of materials for the charged ions. Bethe [27] calculated the S_e using quantum-mechanical perturbation theory, and found the S_e is proportional to the square of the fully ionized charges of the particles. The S_e of the free-electron gas (FEG) model [28] can be expressed as $S_e = Q(Z_1,r_s)v$ in the low-energy range, in which the friction coefficient Q is a function of the atomic number of the projectile, Z_1, and the Wigner-Seitz radius of the FEG, r_s. The FEG model is valid for the S_e of slow ions in metals in which only delocalized conduction electrons are considered to be excited. This has been experimentally confirmed in many materials at ion velocities below Bohr velocity [20,29]. At high velocities, another widely used analytical model is Lindhard-Winther theory [30], which describes the S_e via the dielectric function for the FEG model:

$$S(Z_1, v) = \frac{4\pi {Z_1}^2 e^4}{m_e v^2} n_a L(v) \tag{1}$$

where Z_1 is the atomic number of the projectile ion, v is the ion velocity, and n_a is the electron density of the FEG model. $L(v)$ is a velocity-dependent quantity called the stopping logarithm [31,32]; this quantity is given according to the mean excitation energy of the target material in Bethe theory, or as the energy or wave-vector dependent dielectric response function in the formula of Lindhard and Winther [30]. Unfortunately, the influence of lattice structure and inhomogeneity

*Corresponding author: maofei@mail.bnu.edu.cn
†Corresponding author: gao_congzhang@iapcm.ac.cn

 ©2023 American Physical Society

of electron density is completely ignored by the FEG model or the Lindhard-Winther linear-response model. In addition, the projectile ions are assumed fully stripped and the electron density is input as an external parameter in the two models. In order to accurately describe electronic stopping, lattice structure and electronic structure of host materials as well as charge exchange between ions and host atoms should be considered, and these characteristics become particularly important in the low-energy stopping. The real-time time-dependent density-functional theory (RT-TDDFT) has explicitly taken into account the effects of the inhomogeneity in electron density due to these characteristics. Hence, RT-TDDFT provides a powerful theoretical tool to accurately determine the S_e of a variety of projectile-target combinations, and it provides physical insight into the nonadiabatic behaviors occurring in the electronic stopping at the atomic level.

Recently, the S_e of solids for protons and He ions showed unexpected deviations from velocity proportionality in the low-energy range. The stopping cross section (SCS) of Au [16], Ag, and Cu [17] for protons deviates from the velocity proportionality due to the d-electron excitation at 0.175, 0.19, and 0.2 a.u., respectively. The velocity at which the excitation of d electrons is triggered is called kink velocity. Quashie *et al.* [33] calculated the S_e of copper for protons by performing RT-TDDFT simulations, and the S_e displays a deviation from the velocity proportionality at 0.07 a.u., which is due to the d-electron excitation of Cu. It was also reported that the off-channeling stopping is greatly improved and consistent with the experimental data compared with the channeling stopping. Markin and coworkers studied the electronic energy loss of light ions in insulators with large band gaps at very low velocities, and the SCS of LiF [34] and KCl [35] for H and He ions showed the threshold velocity below which the electronic excitation is prohibited and the electronic stopping vanishes. Recent measurements showed that the SCS of Al [36] and Pt [37] for protons is perfectly proportional to velocity, as expected by the FEG model. However, a distinct departure from the velocity proportionality was observed for He ions in Al [36], and this deviation is interpreted as an additional energy-loss channel due to the complex electronic structure of He ions and the charge exchange between He and aluminum atoms in close encounters.

At high velocities, the electronic energy loss of ions is mainly due to the excitation of inner-shell electrons of the host materials. Lohmann and Primetzhofer [3] measured the electronic energy loss of protons and He ions transmitting through single-crystalline silicon in both channeling and off-channeling geometries; the relative contribution of the core electron excitation to the electronic stopping is given as a function of projectile velocity. Ullah *et al.* [1] studied the S_e of self-irradiated Ni, and revealed the importance of core electron excitation of target atoms, especially in the high-energy regime. Ojanperä *et al.* [38] calculated the electronic energy loss of ions traversing the graphene target and indicated that accounting for core electron excitations of both projectile and target atoms is crucial for a quantitative description of the S_e. Yao *et al.* [39] calculated the S_e of water for protons and pointed out the K-shell core electron excitation of oxygen atoms was found to be pivotal in determining the S_e beyond its maximum. These results indicate that the contribution of core electron excitation and off-channeling incidence geometry should be considered in theoretical investigation to improve the S_e. Bergsmann *et al.* [40] studied the stopping of protons and He ions in Mg, and the results showed that the SCS for He ions is higher than that predicted by the FEG model considering only conduction electrons; this discrepancy was assumed to be caused by the electron promotion which is due to the overlap between He $1s$ and Mg $2p$ orbitals, and the excitation of the inner-shell electrons of Mg.

In this paper, we present RT-TDDFT calculation of S_e of Mg for protons and He ions moving along both midpoint and off-channeling trajectories. We focus on the threshold velocity for $2p$-electron excitation of Mg in the low-energy region and the contribution of $2p$-electron excitation to the S_e in the high-energy region. Finally, the charge state of protons and He ions is calculated, and validity of linear-response theory to describe the S_e of Mg is examined.

II. METHOD AND COMPUTATIONAL DETAILS

To study the physical mechanism for the electronic energy loss of ions in magnesium, the RT-TDDFT combined with molecular-dynamics [41–43] scheme is employed to calculate the S_e of Mg for protons and He ions. This scheme makes it possible to study the nonequilibrium response of the electronic subsystem of the media under ion irradiation, and RT-TDDFT simulations provide physical insights into the role of electronic structure of both the projectile and the target on the S_e [44,45]. The molecular dynamics allows us to study the trajectories of ions in solids in real time.

The time-dependent Kohn-Sham equations are employed to describe the evolution of the energy of the system (atomic units are used hereafter):

$$i\frac{\partial\varphi_i(\mathbf{r},t)}{\partial t}=\left[-\frac{1}{2}\nabla^2+V_{\mathrm{KS}}[n,\{\mathbf{R}_J(t)\}](\mathbf{r},t)\right]\varphi_i(\mathbf{r},t), \quad (2)$$

where $\mathbf{R}_J(t)$ is the time-dependent position of the nuclei. The electronic states are evolved in time with a self-consistent Hamiltonian that is a functional of electron density. The Kohn-Sham effective potential $V_{\mathrm{KS}}[n,\{\mathbf{R}_J\}](\mathbf{r},t)$ is given by

$$V_{\mathrm{KS}}[n,\{\mathbf{R}_J\}](\mathbf{r},t)=V_{\mathrm{ext}}[\{\mathbf{R}_J\}](\mathbf{r},t)+V_{\mathrm{H}}[n](\mathbf{r},t)+V_{\mathrm{XC}}[n](\mathbf{r},t), \quad (3)$$

in which $V_{\mathrm{ext}}(\mathbf{r},t)$ is the time-dependent electron-nucleus potential, $V_{\mathrm{H}}[n](\mathbf{r},t)$ is the Hartree potential which describes the classical electrostatic interaction between electrons, and $V_{\mathrm{XC}}[n](\mathbf{r},t)$ presents the time-dependent exchange-correlation potential. The electron density of the system is given by

$$n(\mathbf{r},t)=2\sum_i|\varphi_i(\mathbf{r},t)|^2. \quad (4)$$

In this paper, the bulk Mg is modeled by a $3\times3\times3$ hexagonal close-packed supercell containing 54 atoms, with periodic boundary conditions along with Ewald summation [46] being employed in three dimensions throughout this paper. The interaction between the valence electrons and the ionic cores for both Mg atoms and the projectile ions is described by the norm-conserving Troullier-Martins

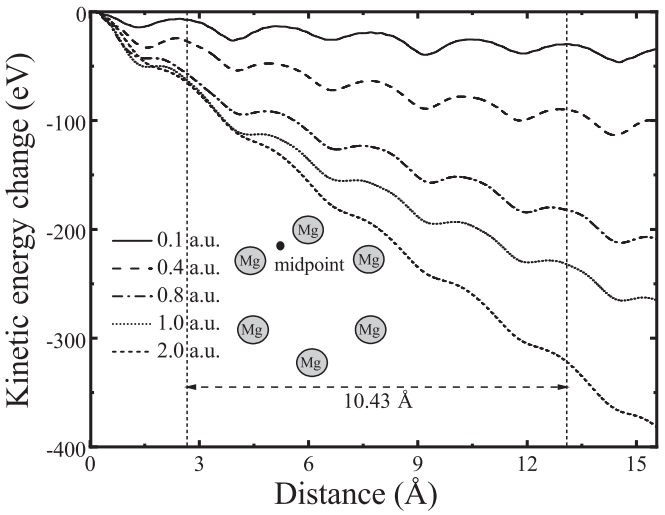

FIG. 1. The kinetic-energy change as a function of the displacement of He ions traveling along the midpoint trajectory. The inset shows the top view of the incidence geometry. The gray circles represent the magnesium atoms, and the black circle indicates the impact location of the projectiles.

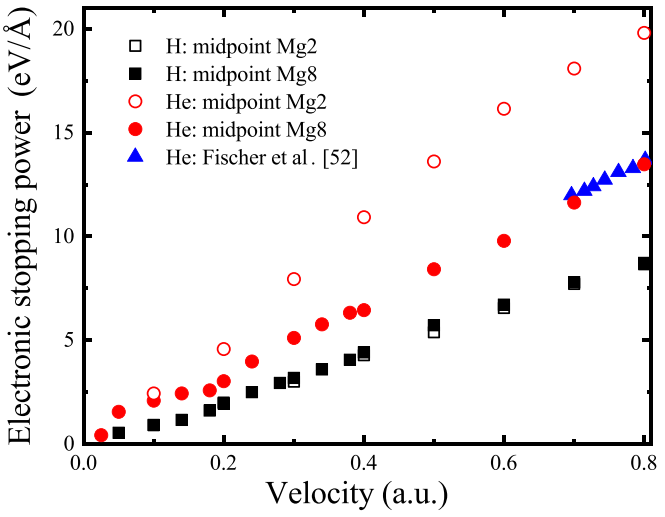

FIG. 2. Electronic stopping power of magnesium for protons and He ions moving along the midpoint trajectory obtained from Mg2 and Mg8 pseudopotential models as a function of velocity. Experimental data from Ref. [52] are also presented.

pseudopotential [47]. The adiabatic local-density approximation (ALDA) with Perdew-Wang parametrization [48] is adopted for the exchange-correlation potential. Only one k point (Γ) is sampled in the Brillouin zone of the supercell. The wave functions, electron densities, and external potentials are discretized in a real-space grid with uniform spacing of 0.16 Å along all three spatial coordinates in the simulation cell, which has been checked to yield well-converged S_e. To investigate the threshold velocity of $2p$-electron excitation and its contribution to the S_e of Mg explicitly, two pseudopotentials were constructed for the Mg atom. One pseudopotential containing two electrons in the valence electron configuration is referred to as Mg2 ([Ne]$3s^2$), and the other one containing eight electrons is referred to as Mg8 ([He$2s^2$]$2p^6 3s^2$). The contribution of inner $2p$-electron excitation to S_e is revealed by comparing the S_e obtained from the two pseudopotential models.

In the time-dependent evolution, the projectile is originally placed on the boundary of the simulation box, and an initial velocity is given instantaneously at the beginning of the time evolution simulations. All Mg atoms are fixed at their equilibrium positions in the time-dependent simulations [32,33]. Therefore, the nuclear stopping can be ignored during the stopping process. The kinetic energy of the projectiles is gradually deposited into the electronic subsystem of Mg through inelastic collisions with host atoms as the projectiles are moving in the midpoint trajectory and off-channeling geometries. The trajectories of the ions are integrated by the Verlet algorithm, and the approximated enforced time-reversal symmetry method is employed for propagating the electronic wave functions with a certain step length so that $\Delta t \times v \approx 2.4 \times 10^{-3}$ Å (except for the case of 0.05 a.u. which is 1.2×10^{-3} Å), which is used to ensure the convergence of the total energy. In the midpoint geometry, the projectiles move along the c axis of Mg and the incident point is shown in the insets of Fig. 1. The instantaneous S_e is defined as the energy-loss rate of the projectile kinetic energy $E(x)$ with respect to projectile displacement x, $S_e = -dE(x)/dx$.

Figure 1 shows the kinetic-energy change as a function of the displacement of He ions traveling along the midpoint trajectory at different velocities. The oscillation of the kinetic-energy loss displays the periodicity of the lattice structure. It is important to note that the charge state of the projectile is not controlled externally, but it is part of the RT-TDDFT calculations. Notably, the sudden movement of the projectiles and the capture of electrons from the host atoms at the beginning of time-dependent evolution result in a "transient" on the kinetic-energy loss before the ions reach the equilibrium charged state. In order to eliminate the influence of this transient on the accuracy of the S_e, the S_e is extracted after the projectiles have achieved the equilibrium charge state. The equilibrium S_e is obtained by averaging the instantaneous S_e over the two lattice periods [49] between the two vertical dashed lines, as indicated in Fig. 1.

For the off-channeling geometry, four incident points and three incident directions for each incident point are randomly sampled for the projectiles; each incident direction is described by a unit direction vector which is generated by random numbers. As many impact parameters as possible are probed by each off-channeling trajectory, and the head-on-head collision is avoided in the off-channeling trajectories, so there are 12 off-channeling trajectories at each velocity. The off-channeling S_e is obtained by averaging the stopping power over the 12 off-channeling trajectories for each velocity. All calculations are performed by the OCTOPUS code [50,51].

III. RESULTS AND DISCUSSION

The S_e of Mg for protons and He ions traveling along the midpoint trajectory for ion velocities ranging from 0.1 to 0.8 a.u. is shown in Fig. 2. The figure also holds experimental stopping data [52] for He ions. The S_e of protons obtained

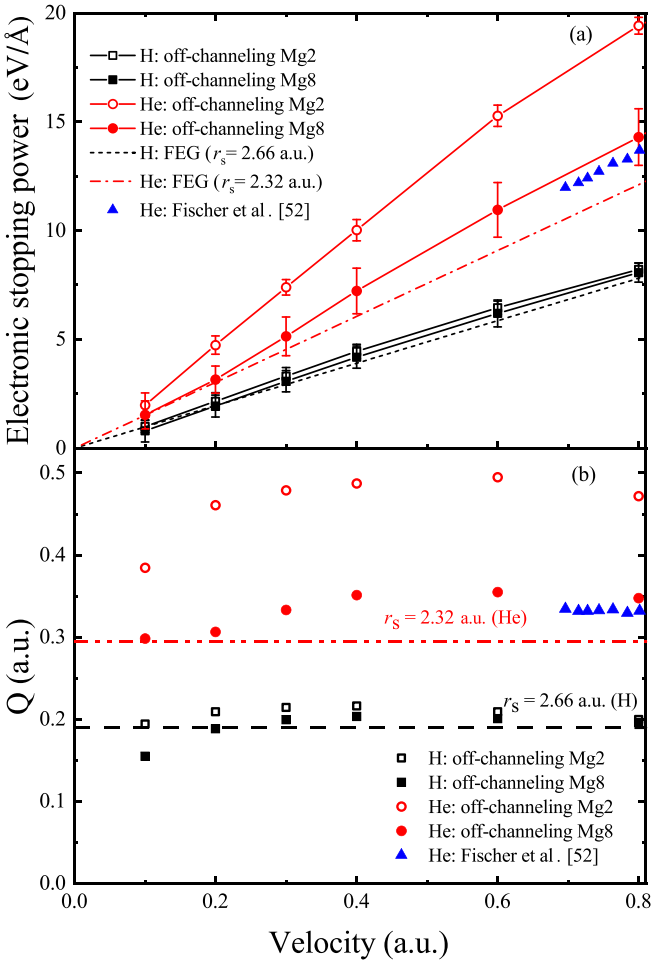

FIG. 3. (a) The off-channeling stopping power of Mg for protons and He ions as a function of velocity. (b) The corresponding friction coefficient Q is shown as a function of velocity. Experimental data [52] along with FEG predictions based on DFT calculation for H [53] and He [54,55] ions are also displayed.

from Mg2 and Mg8 pseudopotentials do not differ much in the low-energy region, indicating that the 3s electron is sufficient to describe the S_e of protons moving along the midpoint trajectory in the low-velocity regime. For He ions, the S_e obtained from the Mg8 pseudopotential is in a good agreement with the experimental data [52], while the S_e obtained from Mg2 pseudopotential rises with a higher slope. A comparison of the S_e obtained from the two pseudopotentials shows that the addition of the 2p electron reduces the S_e of He ions in the low-energy range; the reason will be discussed later.

Figure 3 shows the off-channeling S_e obtained from Mg2 and Mg8 pseudopotential models in the low-energy range, along with the FEG predictions with Wigner-Seitz radius $r_s = 2.66$ ($3s^2$) and 2.32 a.u. ($2p^1 3s^2$), which corresponds to two and three electrons per Mg atom, respectively. For protons, our off-channeling stopping obtained from the Mg8 pseudopotential is consistent with the FEG result with $r_s = 2.66$ a.u. in the low velocity range. For He ions, the off-channeling S_e obtained from the Mg8 pseudopotential is consistent with the FEG predictions with $r_s = 2.32$ a.u. at $v \leqslant 0.2$ a.u. The S_e of He ions predicted by the FEG model

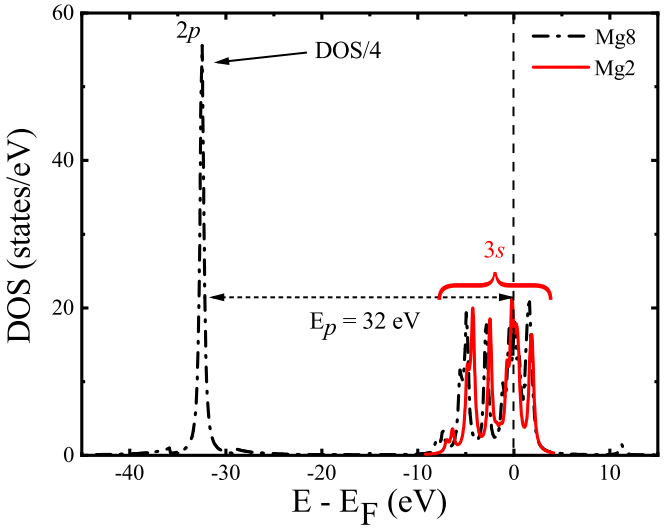

FIG. 4. The electronic density of states of Mg. The Fermi energy is shifted to zero and the high values due to the 2p band are scaled down by a factor of 4.

including eight electrons is much higher than our calculation, which suggests that only partial 2p inner electrons are excited in the low-energy range and the excitation of 2p electrons is a gradual process. The corresponding friction coefficient Q for protons and He ions is shown in Fig. 3(b). For protons, the off-channeling Q obtained from the Mg8 pseudopotential increases gradually to the FEG prediction considering only 3s electrons ($r_s = 2.66$ a.u.) at $v < 0.2$ a.u., and the Q values are in line with the FEG predictions including only the 3s electron at $v \geqslant 0.2$ a.u. It can be derived that the 2p electrons are not excited in the low velocity region. Although the off-channeling Q obtained from the Mg2 pseudopotential is consistently higher than that in the Mg8 pseudopotential at $v < 0.8$ a.u., the differences between the two pseudopotentials is gradually decreasing as the velocity increases. It means that the introduction of the 2p electron suppresses the excitation of the 3s electron, which is commonly known as the "shake-up" effect [39]. For He ions, the shake-up effect shows up more pronouncedly, and the off-channeling Q values obtained from the Mg8 pseudopotential are in line with the experimental data [52]. The off-channeling S_e of He ions showed that 2p electrons are excited beginning at 0.1 a.u.

The electronic DOS of Mg is shown in Fig. 4. The energy distribution of the 3s band and the inner 2p band can be distinguished by comparing the DOS results obtained from the two pseudopotential models. As shown in Fig. 4, the occupied 2p states of Mg are located at about 32 eV below the Fermi level. Consequently, the threshold velocity for excitation of the 2p electron to the Fermi level can be calculated by the following equation [33]:

$$v_k = \frac{E_p}{2\hbar k_F}, \tag{5}$$

where $E_p = 32$ eV, and the Fermi wave vector $k_F = 1.92/r_s = 0.72/a_0$ is for the FEG containing only 3s electrons of Mg ($r_s = 2.66$ a.u.). The calculated kink velocity $v_k = 0.82$ a.u. for both protons and He ions according to Eq. (5). Thus, one

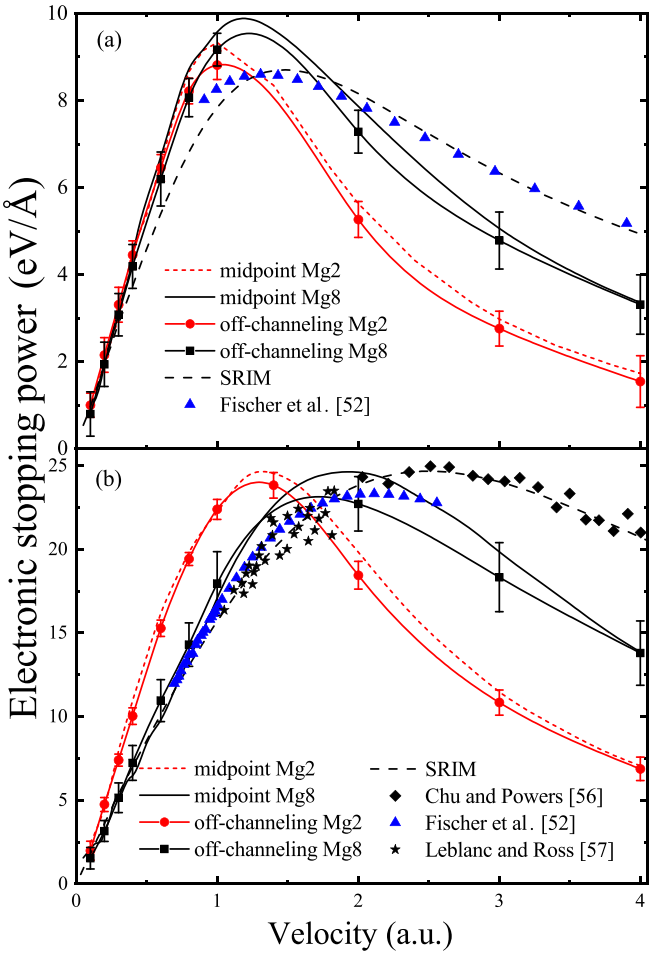

FIG. 5. The electronic stopping power of Mg for (a) H^+ and (b) He^{2+} ions as a function of velocity. The red and black lines indicate the S_e obtained from Mg2 and Mg8 pseudopotentials in the midpoint trajectory, respectively. The red circles and black squares represent the off-channeling S_e within the two pseudopotential models, respectively. The black dashed line corresponds to the tabulated stopping of the SRIM package [58]. Experimental data from Refs. [52,56,57] are presented.

may assume that the $2p$ electrons do not participate in the electronic stopping dynamics at $v < 0.82$ a.u. For protons, it can be seen from Fig. 3 that $2p$ electrons are not excited under the off-channeling condition below 0.8 a.u., which is consistent with the calculated result from Eq. (5). For He ions, the $2p$ electrons are excited at $v = 0.1$ a.u. in the off-channeling condition.

Figure 5 presents calculated S_e of Mg for protons and He ions in comparison with experimental measurements [52,56,57] and SRIM predictions [58] in the velocity range of $0.1 < v < 4.0$ a.u. For the Mg8 pseudopotential, there are some discrepancies in the S_e between the midpoint and off-channeling geometries, suggesting that the contribution of $2p$-electron excitation to S_e is particularly sensitive to the impact parameter. The S_e including also the $2p$ electrons is greatly improved beyond the stopping maximum compared to those obtained from the Mg2 pseudopotential for both midpoint and off-channeling trajectories, thereby verifying that it is crucial to consider the contribution of $2p$-electron excitation to obtain a reasonable S_e at high velocities. For the Mg2 pseudopotential, there are some minor differences in the S_e between the midpoint and off-channeling geometries, indicating that the contribution of $3s$-electron excitation to S_e is related to the impact parameter when the protons approach the Mg nuclei. As shown in Fig. 5(a), the off-channeling S_e of protons obtained from Mg2 and Mg8 is consistent with the measured data [52] up to the stopping maximum, but lower than the experimental data [52] beyond 1.4 and 1.7 a.u., respectively. Making a comparison between the off-channeling S_e obtained from Mg2 and Mg8 pseudopotentials, as shown in Fig. 5(a), it is found that the excitation of $2p$ electrons is triggered at $v > 0.8$ a.u., which is consistent with the static calculation of the kink velocity.

For He ions, it can be seen from Fig. 5(b) that the agreement between the off-channeling S_e including also the $2p$ electron and the measured data is achieved up to 1.8 a.u. The off-channeling S_e including also $2p$-electron excitation is increased by 50.2% at $v = 4.0$ a.u. compared to the off-channeling S_e considering only valance electrons. In addition, the introduction of $2p$ electrons shifts the stopping maximum position of both midpoint and off-channeling trajectories towards higher velocities. In general, the off-channeling S_e of both protons and He ions quantitatively underestimates the experimental data beyond the stopping maximum, which may be improved by incorporating more inner electrons in the electronic stopping at higher velocities. For both protons and He ions, the S_e obtained in the midpoint trajectory is consistent with that obtained in the off-channeling geometry for both Mg2 and Mg8 pseudopotentials, except at the stopping maximum position of He ions in the Mg8 pseudopotential, just as the S_e of the "centroid path" represents well for the off-channeling stopping of SiC [32].

Linear-response theory predicts a quadratic dependence of the S_e on the charge state of a fully stripped projectile, which neglects the charge capture ability of the projectile. However, previous numerical studies [59–61], to some extent, have revealed that the charge transfer between the projectiles and the host atoms might be an important energy-loss channel for slow ions. For this reason, it is instructive to study the effect of ion charge state on S_e. We explored whether the description can be improved by using the velocity dependent charge state of projectiles from our nonequilibrium simulations rather than assuming fully ionized projectiles. The mean steady-state charge of the projectiles moving along the midpoint trajectories is calculated in our RT-TDDFT simulation. The electron density captured by the projectiles is regarded as spherically distributed. The space around the midpoint ions is divided into different spherical shells depending on the radius, in which the shell thickness is set to be 0.1 Å. The electron density in these spherical shells is calculated, and the electron density of the shells decreases to the minimum with increasing the radius of the shell. The radius of the shell with the lowest electron density is regarded as the border of the electron density between the projectiles and Mg atoms, which is adopted as the integration radius for calculating the charges captured by the projectiles. Using the above method, the radius that we choose for integrating the ion charge is 0.6 Å for both protons and He ions.

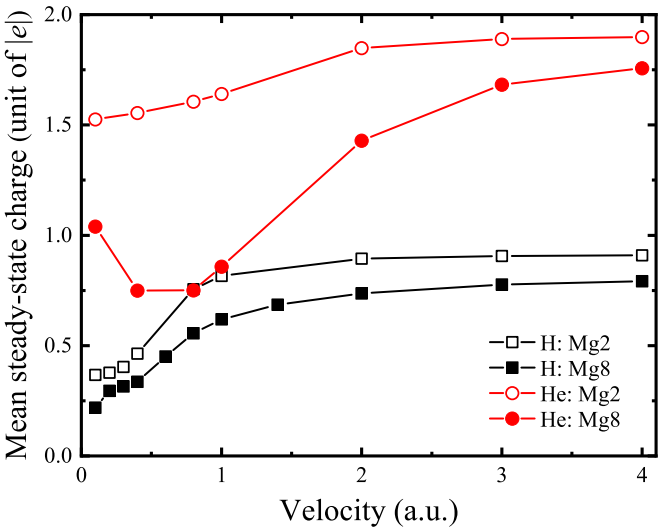

FIG. 6. The mean steady-state charge of protons and He ions traveling in the midpoint trajectory as a function of velocity.

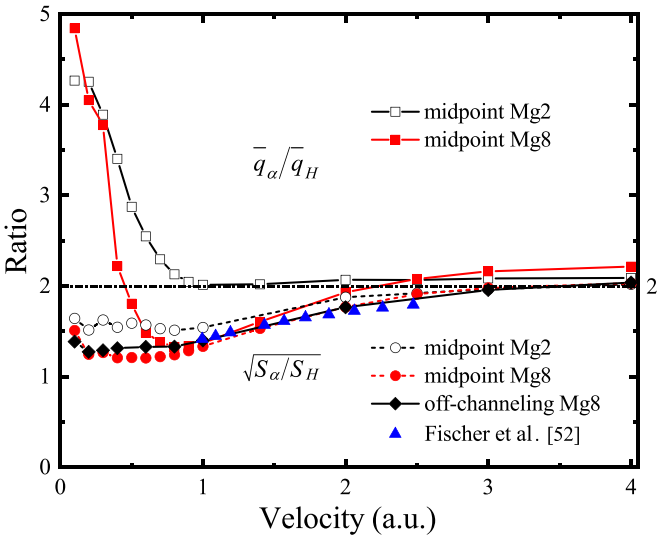

FIG. 7. Velocity-dependent ratios between He ions and protons for stopping power and mean steady-state charge in magnesium. Squares and circles show the $\overline{q}_\alpha/\overline{q}_H$ and the $\sqrt{S_\alpha/S_H}$ obtained from the midpoint trajectory, respectively. Full and open symbols indicate the results with $2p$ electrons considered or not, respectively. Diamond and triangle symbols represent the $\sqrt{S_\alpha/S_H}$ calculated from off-channeling trajectories and derived from the experimental data, respectively. Within linear-response theory, the $\sqrt{S_\alpha/S_H}$ equals to 2 as represented by the dash-dotted line if fully ionized projectiles are assumed.

The mean steady-state charge of the projectiles obtained from our nonequilibrium RT-TDDFT simulations is shown in Fig. 6. As expected, the charge of the projectiles increases with the ion velocity, and the projectiles can be considered as bare ions at $v > 4.0$ a.u. The results should not be regarded as a quantitative prediction, since the ALDA employed in our calculations is local in time and space, and it cannot give an exact description for the electron exchange occurring in the collisions. The deviations of the S_e of He ions from the velocity proportionality in the low-energy region can be ascribed to the charge exchange effect between He ions and Mg, which is considered as an important additional energy-loss channel for slow ions. It is noted that the mean steady-state charge for He ions obtained from the Mg2 model is much higher than that obtained from the Mg8 model at $v < 1.5$ a.u., especially at low velocities (i.e., the calculated mean steady-state charge obtained from the Mg2 pseudopotential is higher than that of the Mg8 pseudopotential by 53% at 0.8 a.u.). It gives rise to the S_e considering only the valence electron is higher than that including also the $2p$ electron for $v < 1.4$ a.u. in the midpoint trajectory, as shown in Fig. 5(b).

To further examine the impact of the ion charge state on the S_e, the effective charge state for the α particle, $\sqrt{S_\alpha/S_H}$, and the mean steady-state charge ratio, $\overline{q}_\alpha/\overline{q}_H$, are quantified; the results are shown in Fig. 7. For the midpoint trajectory, our simulation results and experimental data showed that $\sqrt{S_\alpha/S_H}$ is less than 2 for $v < 3.0$ a.u., and it converges at 2 beyond 3.0 a.u., as one would expect from assuming fully ionized projectiles in the linear-response theory. However, the $\sqrt{S_\alpha/S_H}$ given by the Mg2 pseudopotential model is higher than that given by the Mg8 pseudopotential model in the midpoint geometry at $v \leqslant 2.5$ a.u. Likewise, the $\overline{q}_\alpha/\overline{q}_H$ obtained from the Mg2 pseudopotential is higher than that obtained from the Mg8 pseudopotential in the midpoint geometry at $v < 2.5$ a.u., except for at extremely low velocity of 0.1 a.u. It is noted that $\overline{q}_\alpha/\overline{q}_H$ obtained from the Mg2 pseudopotential converges rapidly toward 2 in the midpoint geometry at $v \geqslant 1.0$ a.u., which is distinctly different from that observed for the Mg8 pseudopotential. For the Mg2 pseudopotential, the $\sqrt{S_\alpha/S_H}$ and the $\overline{q}_\alpha/\overline{q}_H$ are basically in agreement beyond 2.5 a.u. For the Mg8 pseudopotential, the two quantities are in good agreement even at low ion velocities down to 0.8 a.u. For the off-channeling trajectory, our calculations showed that the $\sqrt{S_\alpha/S_H}$ reaches 2 beyond 3.0 a.u., and it is consistent with the experimental data down to 1.0 a.u. Consequently, this suggests that the scaling relationship $\sqrt{S_\alpha/S_H} = \overline{q}_\alpha/\overline{q}_H$ can be extended to low velocities provided that the mean steady-state charge is employed instead of assuming fully ionized charges and considering also $2p$-electron excitation of Mg.

IV. CONCLUSIONS

In conclusion, we studied the S_e of Mg for protons and He ions by real-time time-dependent density-functional theory combined with molecular-dynamics simulation. The effects of p-electron excitation on the S_e of Mg are clarified. The threshold effect for the S_e of protons is found in the off-channeling geometry, and the threshold velocity is at $v > 0.8$ a.u. The off-channeling S_e of He ions showed that the $2p$ electron is excited down to $v = 0.1$ a.u., and that the S_e deviates from the velocity proportionality, which can be ascribed to the additional energy loss caused by the charge exchange between He ions and host electrons. Our results displayed that the S_e is greatly enhanced by p-electron excitation at small impact parameters.

Our off-channeling S_e including also inner $2p$ electrons is greatly improved and it is in a good agreement with the

experimental data up to 1.8 a.u. for He ions. Our results showed that $2p$-electron excitation dominates the S_e of Mg beyond the stopping maximum, and more core electrons are needed to be considered to predict the measured S_e in the high-energy region. In addition, by quantifying the mean steady-state charge of protons and He ions, we examined the extent to which the linear-response theory is applicable to describe the S_e. The results showed that the validity of the scaling relationship $\sqrt{S_\alpha/S_H} = \bar{q}_\alpha/\bar{q}_H$ can be extended to lower velocities if the mean steady-state charge is employed instead of assuming fully ionized projectiles as well as considering also the $2p$-electron excitation of Mg.

ACKNOWLEDGMENT

This work is supported by the National Natural Science Foundation of China under Grants No. 11975119, No. 11774030, and No. 12135004.

[1] R. Ullah, E. Artacho, and A. A. Correa, Phys. Rev. Lett. **121**, 116401 (2018).
[2] A. E. Sand, R. Ullah, and A. A. Correa, npj Comput. Mater. **5**, 43 (2019).
[3] S. Lohmann and D. Primetzhofer, Phys. Rev. Lett. **124**, 096601 (2020).
[4] R. C. Fadanelli, C. D. Nascimento, C. C. Montanari, J. C. Aguiar, D. Mitnik, A. Turos, E. Guziewicz, and M. Behar, Eur. Phys. J. D **70**, 178 (2016).
[5] X. Qi, F. Bruneval, and I. Maliyov, Phys. Rev. Lett. **128**, 043401 (2022).
[6] D. Jedrejcic and U. Greife, Nucl. Instrum. Methods Phys. Res. Sect. B **428**, 1 (2018).
[7] P. L. Grande, Phys. Rev. A **94**, 042704 (2016).
[8] K. G. Reeves, Y. Yao, and Y. Kanai, Phys. Rev. B **94**, 041108(R) (2016).
[9] P. K. Patel, A. J. Mackinnon, M. H. Key, T. E. Cowan, M. E. Foord, M. Allen, D. F. Price, H. Ruhl, P. T. Springer, and R. Stephens, Phys. Rev. Lett. **91**, 125004 (2003).
[10] G. S. Was, *Fundamentals of Radiation Material Science* (Springer-Verlag, Berlin, 2007).
[11] E. A. Figueroa, E. D. Cantero, J. C. Eckardt, G. H. Lantschner, J. E. Valdés, and N. R. Arista, Phys. Rev. A **75**, 010901(R) (2007).
[12] D. Schardt, T. Elsässer, and D. Schulz-Ertner, Rev. Mod. Phys. **82**, 383 (2010).
[13] J. Lindhard, M. Scharff, and H. E. Schiøtt, Mat. Fys. Medd. Dan. Vid. Selsk. **33**, no. 14 (1963).
[14] M. T. Robinson and I. M. Torrens, Phys. Rev. B **9**, 5008 (1974).
[15] K. Arstila, J. Keinonen, P. Tikkanen, and A. Kuronen, Phys. Rev. B **43**, 13967 (1991).
[16] S. N. Markin, D. Primetzhofer, M. Spitz, and P. Bauer, Phys. Rev. B **80**, 205105 (2009).
[17] D. Goebl, D. Roth, and P. Bauer, Phys. Rev. A **87**, 062903 (2013).
[18] J. E. Valdés, J. C. Eckardt, G. H. Lantschner, and N. R. Arista, Phys. Rev. A **49**, 1083 (1994).
[19] J. E. Valdés, G. Martínez Tamayo, G. H. Lantschner, J. C. Eckardt, and N. R. Arista, Nucl. Instrum. Methods Phys. Res. Sect. B **73**, 313 (1993).
[20] R. Blume, W. Eckstein, H. Verbeek, and K. Reichelt, Nucl. Instrum. Methods Phys. Res. **194**, 67 (1982).
[21] E. D. Cantero, G. H. Lantschner, J. C. Eckardt, and N. R. Arista, Phys. Rev. A **80**, 032904 (2009).
[22] M. Inokuti, Rev. Mod. Phys. **43**, 297 (1971).
[23] P. E. Grabowski, M. P. Surh, D. F. Richards, F. R. Graziani, and M. S. Murillo, Phys. Rev. Lett. **111**, 215002 (2013).
[24] E. Rutherford, Edinburgh Dublin Philos. Mag. J. Sci. **21**, 669 (1911).
[25] J. J. Thomson, Edinburgh Dublin Philos. Mag. J. Sci. **23**, 449 (1912).
[26] C. G. Darwin, Edinburgh Dublin Philos. Mag. J. Sci. **23**, 901 (1912).
[27] H. Bethe, Ann. Phys. (NY) **397**, 325 (1930).
[28] E. Fermi and E. Teller, Phys. Rev. **72**, 399 (1947).
[29] P. M. Echenique, F. Flores, and R. H. Ritchie, Solid State Phys. **43**, 229 (1990).
[30] J. Lindhard and A. Winther, Mat. Fys. Medd. Dan. Vid. Selsk. **34**, no. 4 (1964).
[31] C.-W. Lee, J. A. Stewart, R. Dingreville, S. M. Foiles, and A. Schleife, Phys. Rev. B **102**, 024107 (2020).
[32] D. C. Yost and Y. Kanai, Phys. Rev. B **94**, 115107 (2016).
[33] E. E. Quashie, B. C. Saha, and A. A. Correa, Phys. Rev. B **94**, 155403 (2016).
[34] M. Draxler, S. P. Chenakin, S. N. Markin, and P. Bauer, Phys. Rev. Lett. **95**, 113201 (2005).
[35] S. N. Markin, D. Primetzhofer, and P. Bauer, Phys. Rev. Lett. **103**, 113201 (2009).
[36] D. Primetzhofer, S. Rund, D. Roth, D. Goebl, and P. Bauer, Phys. Rev. Lett. **107**, 163201 (2011).
[37] C. E. Celedón, E. A. Sánchez, L. S. Alarcón, J. Guimpel, A. Cortés, P. Vargas, and N. R. Arista, Nucl. Instrum. Methods Phys. Res. Sect. B **360**, 103 (2015).
[38] A. Ojanperä, A. V. Krasheninnikov, and M. Puska, Phys. Rev. B **89**, 035120 (2014).
[39] Y. Yao, D. C. Yost, and Y. Kanai, Phys. Rev. Lett. **123**, 066401 (2019).
[40] M. Bergsmann, P. Hörlsberger, F. Kastner, and P. Bauer, Phys. Rev. B **58**, 5139 (1998).
[41] X. Andrade, A. Castro, D. Zueco, J. L. Alonso, P. Echenique, F. Falceto, and A. Rubio, J. Chem. Theory Comput. **5**, 728 (2009).
[42] J. L. Alonso, X. Andrade, P. Echenique, F. Falceto, D. Prada-Gracia, and A. Rubio, Phys. Rev. Lett. **101**, 096403 (2008).
[43] A. Castro, M. Isla, J. I. Martínez, and J. A. Alonso, Chem. Phys. **399**, 130 (2012).
[44] D. R. Mason, J. L. Page, C. P. Race, W. M. C. Foulkes, M. W. Finnis, and A. P. Sutton, J. Phys.: Condens. Matter **19**, 436209 (2007).
[45] M. A. Zeb, J. Kohanoff, D. Sánchez-Portal, and E. Artacho, Nucl. Instrum. Methods Phys. Res. Sect. B **303**, 59 (2013).
[46] T. Amisaki, J. Comput. Chem. **21**, 1075 (2000).
[47] N. Troullier and J. L. Martins, Phys. Rev. B **43**, 1993 (1991).
[48] J. P. Perdew and Y. Wang, Phys. Rev. B **45**, 13244 (1992).
[49] S.-M. Li, F. Mao, X.-D. Zhao, B.-S. Li, W.-Q. Jin, W.-Q. Zuo, F. Wang, and F.-S. Zhang, Phys. Rev. B **104**, 214104 (2021).

[50] M. A. L. Marques, A. Castro, G. F. Bertsch, and A. Rubio, Comput. Phys. Commun. **151**, 60 (2003).
[51] X. Andrade, D. A. Strubbe, U. De Giovannini, A. H. Larsen, M. J. T. Oliveira, J. Alberdi-Rodriguez, A. Varas, I. Theophilou, N. Helbig, M. Verstraete, L. Stella, F. Nogueira, A. AspuruGuzik, A. Castro, M. A. L. Marques, and A. Rubio, Phys. Chem. Chem. Phys. **17**, 31371 (2015).
[52] P. Fischer, Ch. Eppacher, G. Höifler, and D. Semrad, Nucl. Instrum. Methods Phys. Res. B **115**, 27 (1996).
[53] J. I. Juaristi, M. Alducin, R. D. Muiño, H. F. Busnengo, and A. Salin, Phys. Rev. Lett. **100**, 116102 (2008).
[54] I. Nagy and A. Arnau, Phys. Rev. B **49**, 9955 (1994).
[55] M. J. Puska and R. M. Nieminen, Phys. Rev. B **27**, 6121 (1983).
[56] W. K. Chu and D. Powers, Phys. Rev. **187**, 478 (1969).
[57] L. Leblanc and G. G. Ross, Nucl. Instrum. Meth. Phys. Res. B **90**, 54 (1994).
[58] J. F. Ziegler, M. Ziegler, and J. Biersack, Nucl. Instrum. Methods Phys. Res. Sect. B **268**, 1818 (2010).
[59] A. Kononov and A. Schleife, Phys. Rev. B **102**, 165401 (2020).
[60] R. Cabrera-Trujillo, J. R. Sabin, Y. Öhrn, and E. Deumens, Phys. Rev. Lett. **84**, 5300 (2000).
[61] R. A. Wilhelm, E. Gruber, V. Smejkal, S. Facsko, and F. Aumayr, Phys. Rev. A **93**, 052708 (2016).